Chin. J. Astron. Astrophys. Vol. 1, No. 5, (2001) 460–468
(http://www.chjaa.org or http://chjaa.bao.ac.cn)

Chinese Journal of
Astronomy and
Astrophysics

Physical Parameters of a Flare Derived from Multi-line 2D Spectroscopy

Ying Liu and Ming-De Ding⋆

Department of Astronomy, Nanjing University, Nanjing 210093

Received 2001 May 21; accepted 2001 June 4

Abstract Time series of 2D spectra of Hα and Ca II λ8542 for a flare of 1999 December 22 are obtained and analyzed with a new fitting technique. The method we proposed can simultaneously yield the four parameters: the line source function, the optical thickness at line center, the line-of-sight velocity and the Doppler width. We present the spatial distributions of the physical parameters and their temporal evolutions determined from the 2D spectra. Our results are consistent with the general picture predicted by the flare dynamic models.

Key words: Sun: flares – Sun: chromosphere

1 INTRODUCTION

Ground-based observations of flares reveal relevant signatures at chromospheric levels, whose interpretation plays a crucial role in the identification of the fundamental physical processes responsible for the flare phenomenon. A better understanding of the flare phenomenon requires multi-line observations and 2D spectroscopy, which can reveal the dynamic behavior of flares at different locations and at different depths.

The most obvious feature of line profiles for solar flares is the red asymmetry, which has been interpreted as a consequence of downflows related to chromospheric condensation (e.g., Ichimoto & Kurokawa 1984; Canfield et al. 1987; Canfield & Galey 1987; Fisher 1987; Gan & Fang 1990; Ding et al. 1995; Cauzzi et al. 1996). Besides, the velocity field in a flaring region may represent an important parameter for discriminating between various energy-transfer mechanisms (Fisher et al. 1985). Therefore, an adequate method for the determination of the velocity field is required. The method most frequently used is the bisector method which was employed by, for example, Ichimoto & Kurokawa (1984), Falchi et al. (1992), and Ding et al. (1995). This method invokes a background profile which is usually hard to determine. Liu & Ding (2001) proposed a new method which avoids the use of background profile, and which allows a simultaneous determination of the four parameters: the line source function, the optical thickness at line center, the line-of-sight velocity and the Doppler width. They obtained some

⋆ E-mail: dmd@nju.edu.cn

preliminary results derived from the Hα line for a flare of 1999 December 22. The results are in qualitative agreement with that predicted by the flare dynamic models.

However, the asymmetry of the chromospheric lines remains to be a puzzling problem. Recent line profile calculations show that a downward motion, when confined to some special circumstances, can also produce a blue asymmetry of the line profiles (e.g., Gan et al. 1993; Ding & Fang 1996, 1997). On the other hand, there appears some evidence showing the existence of a blue asymmetry related to the condensation driven by electron beam heating with the return current (Heinzel et al. 1994). In this work we employ the method proposed by Liu & Ding (2001) to analyze the 2D spectra of Ca II λ8542 for the flare of 1999 December 22 and give insight into the origin of the line asymmetry. The results from Hα have been reported by Liu & Ding (2001). This paper presents the results for Ca II λ8542 and a comparison between this line and Hα.

2 OBSERVATIONS AND DATA REDUCTION

The flare to be analyzed occurred in the active region NOAA 8807 located at N10 E30 on 1999 December 22. The flare began at 01:50 UT, ended at 02:32 UT, and peaked at 02:16 UT. According to the *Solar Geophysical Data*, it is an event with an Hα importance 2B and soft X-ray class M1.8. We have obtained a time series of 2D spectra of the Hα and Ca II λ8542 lines with a CCD imaging spectrograph in the solar tower of Nanjing University using a scanning technique (Huang et al. 1995; Ding et al. 1995). During the flare, we repeated 20 scans over the flaring region from 02:10:00 UT to 02:37:13 UT. Each scan recorded the 2D spectra of the two lines simultaneously. There are 150 pixels with a pixel spacing 0.85″ along the slit, and 50 pixels with a spacing 2″ in the scan direction. The spectrum contains 200 wavelength points with a spectral resolution of 0.05 and 0.118 Å pix^{-1} for the Hα and Ca II λ8542 lines, respectively.

The data reduction includes dark current subtraction and flat field correction for the CCD cameras. The drift of images at different times is also corrected using a cross-correlation procedure. The centers of the Hα and Ca II λ8542 lines are determined from their mean undisturbed profiles near the flaring region by adopting a technique of gaussian fitting.

Figure 1 shows the monochromatic images at the line centers of Hα and Ca II λ8542, reconstructed from the 2D spectra. We concentrate on the spectra within the two kernels displayed in Figure 1, which show conspicuous asymmetries in each of the lines.

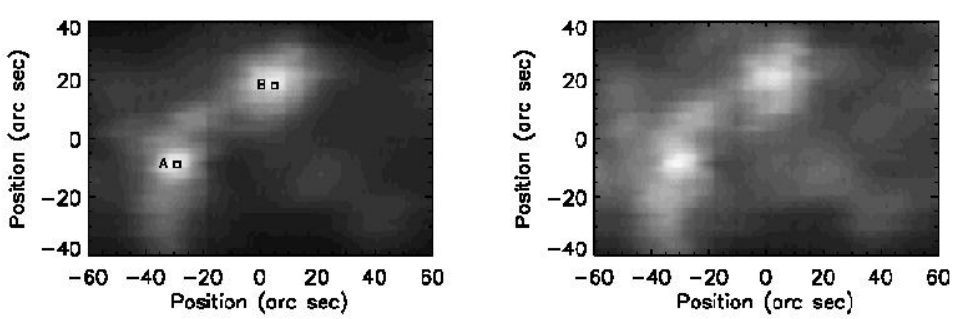

Fig. 1 Monochromatic images of the flare at the Hα line center (left panel), and at the Ca II λ8542 line center (right panel) reproduced from the 2D spectra at 02:09:53 UT. The two small boxes, marked as A and B in the left panel, each cover an area of 1.7″ × 2″.

3 METHOD OF COMPUTATION

We use the same programme proposed by Liu & Ding (2001) to deduce the four parameters: the line source function, S_0, the optical thickness at line center, τ_0, the Doppler shift, $\Delta\lambda_I$ and the Doppler width, $\Delta\lambda_D$, which are all assumed to be constant throughout the perturbed layer in the flare chromosphere. The observed line profile is given by

$$I(\Delta\lambda) = I_0(\Delta\lambda)e^{-\tau(\Delta\lambda)} + S_0[1 - e^{-\tau(\Delta\lambda)}]\,, \tag{1}$$

where S_0 is assumed to be frequency independent, and $I_0(\Delta\lambda)$ is the intensity irradiating the perturbed layer (which is referred to as the layer with a significant downflow) from below. The optical thickness is expressed as

$$\tau(\Delta\lambda) = \tau_0 H(a, x)\,, \tag{2}$$

where $H(a, x)$ is the Voigt profile,

$$H(a, x) = \frac{a}{\pi}\int_{-\infty}^{+\infty} \frac{e^{-y^2}}{a^2 + (x - y)^2}\mathrm{d}y\,, \tag{3}$$

where

$$x = \frac{\Delta\lambda - \Delta\lambda_I}{\Delta\lambda_D}\,, \tag{4}$$

$$a = \frac{\Gamma\lambda_0^2}{4\pi c\Delta\lambda_D}\,. \tag{5}$$

In the above expressions, a is the damping width and Γ the damping constant (We adopt $\Gamma = 1.5 \times 10^8$ s^{-1} for Ca II λ8542).

Below the perturbed layer, the line profile is assumed to be symmetric, that is,

$$I_0(\Delta\lambda) = I_0(-\Delta\lambda)\,. \tag{6}$$

Hence, we define an asymmetry profile as

$$A(\Delta\lambda) \equiv I(\Delta\lambda) - I(-\Delta\lambda) = [I(\Delta\lambda) - S_0][1 - e^{\tau(\Delta\lambda)-\tau(-\Delta\lambda)}]\,. \tag{7}$$

Using the above formulation, we adopt an iterative least square procedure using the Levenberg-Marquardt method to fit the observed asymmetric profile $A(\Delta\lambda)$, instead of the original profile $I(\Delta\lambda)$. Doing so avoids using the profile $I_0(\Delta\lambda)$, which is not known a priori. The computations yield the four unknown parameters S_0, τ_0, $\Delta\lambda_I$, and $\Delta\lambda_D$ mentioned above.

4 DATA ANALYSIS AND RESULTS

The morphology of the flare in Ca II λ8542 is similar to that in Hα (Figure 1), which was also mentioned by Mein et al. (1997). However, the flare appears more diffuse in the case of Ca II λ8542. Both line profiles show conspicuous red asymmetries in the kernels (Figure 1). Liu & Ding (2001) showed, from their result on Hα, that the two kernels are quite similar in their temporal evolution, implying that they are heated by one and the same mechanism.

A typical Ca II λ8542 line profile with red asymmetry is plotted in Figure 2, along with the asymmetry profile defined by Eq. (7). A wavelength window with a reasonable range is selected to exclude the influence of other blended lines. The asymmetry profiles from observations can be well reproduced based on the method. We pick out 6 frames of 2D spectra to investigate the evolution of the parameters, in particular the velocity field. The times of the frames are 02:09:53, 02:11:11, 02:14:03, 02:15:47, 02:17:04 and 02:19:23 UT.

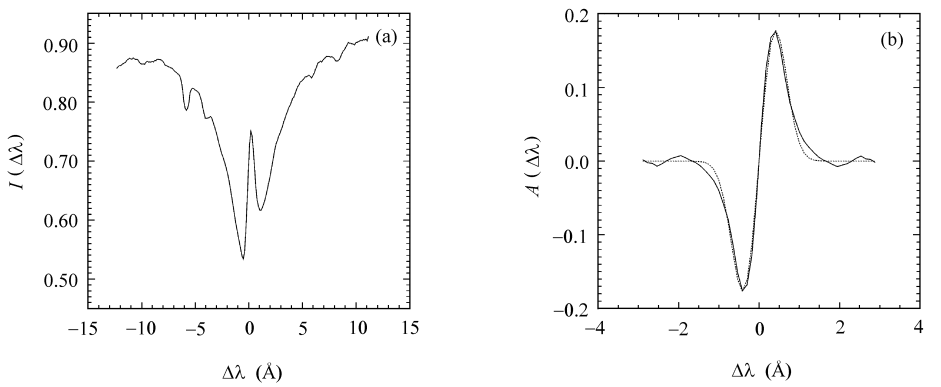

Fig. 2 (a) A typical Ca II λ8542 line profile with red asymmetry in the flare kernels; (b) Comparison between the observed a symmetry profile (solid line) and the fitted one (dotted line). The quantities are normalized to the continuum at 8542 Å.

The four parameters within the kernels are displayed in Figure 3 as contour maps overlying the monochromatic image (the right panel in Figure 1). Over the flare kernels, the properties of the four parameters deduced from Ca II λ8542 are qualitatively similar to the results from Hα (Liu & Ding 2001). Namely, the values are smaller at the edges of the kernels, while enhanced gradually inward. Figure 3c displays a downward velocity with a mean value of about 10 km s^{-1}, smaller than that deduced from Hα (Liu & Ding 2001). Since the height of formation of the Ca II λ8542 line is much lower than that of the Hα line, we can infer that the velocity in the layer contributing to the Ca II λ8542 line emission should be certainly smaller, in the framework where we ascribe the red asymmetry in the present observations as due to the downward propagation of a chromospheric condensation.

Figure 4 displays the temporal evolutions of the four parameters averaged over the ten brightest pixels within the kernels (note that in the time series of observations the flare peaks at 02:15:47 UT, 354 s after the initial time in Figure 4). From Figure 4, we can find a quantitative difference between the parameters derived from the two lines, which may be due to their different processes of formation mentioned above. The temporal evolutions of the parameters, however, are generally similar for the two lines. Such similarities confirm that the two lines should be perturbed by a same heating mechanism and dynamic process, even though they are formed in different circumstances. Figure 4 also shows that the velocity abruptly increased at the onset of the flare, and peaked before the Hα maximum. This picture is also consistent with previous observations (e.g., Ding et al. 1995).

Another interesting feature is that the four parameters show a roughly similar evolution, i.e., they attain their maximum at the onset of the flare, and then decrease. This result is reasonable. When an energetic electron beam hits the flare atmosphere, the source function,

the downward velocity and the Doppler width are increased accordingly; then they should be reduced with the weakening of the electron beam. The optical thickness at the line center, τ_0, is roughly proportional to the column density of hydrogen at the second level, N_2, and inversely proportional to the Doppler width, $\Delta\lambda_D$. Both these two parameters could suffer pronounced changes during this flaring event. However, it is conceivable that the relative change of N_2 dominates over that of $\Delta\lambda_D$, so that τ_0 would vary similarly to the other three parameters.

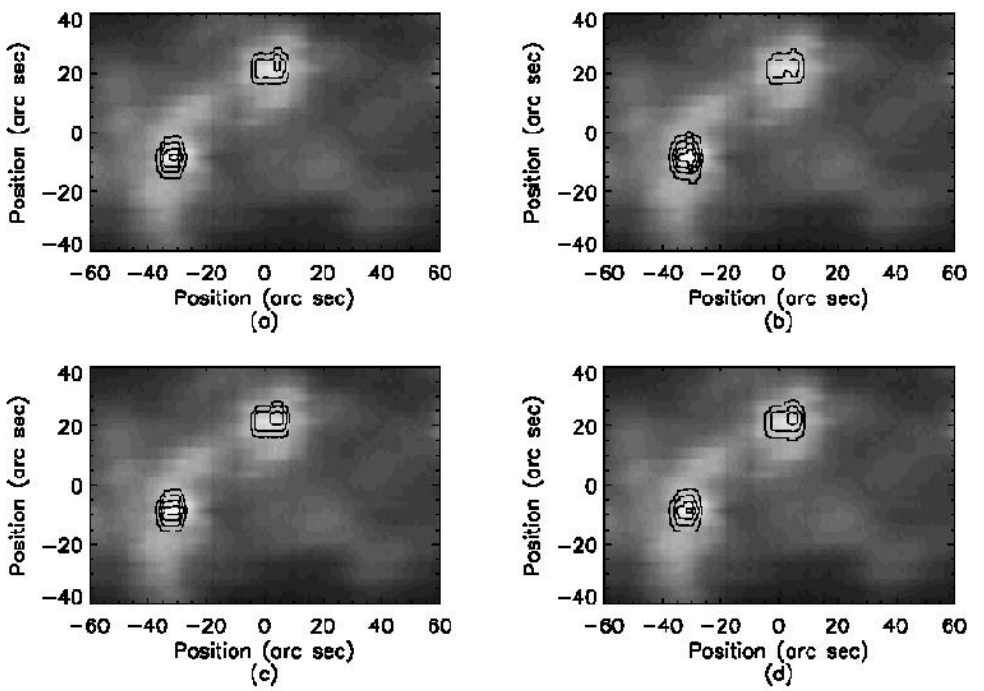

Fig. 3 Contour diagrams of the four parameters within the flare kernels at 02:09:53 UT derived from the Ca II λ8542 profile. (a) source function, contour values: (0.5, 0.7, 0.9, 1.1) $\times I_c$; (b) optical thickness, contour values: (0.15, 0.25, 0.35, 0.45); (c) downward velocity, contour values: (6, 8, 10, 12) km s^{-1}; (d) Doppler width, contour values: (0.25, 0.35, 0.45, 0.55) Å.

To investigate the impact of the condensation on the line profiles, we plot in Figure 5 the mean undisturbed profile near the flaring region, a typical observed profile with red asymmetry, and the intensity profile irradiating the perturbed layer from below, $I_0(\Delta\lambda)$, for Hα and Ca II λ8542, respectively. The last one is constructed from Eq. (1) using the four parameters derived above. $I_0(\Delta\lambda)$ is symmetric just as assumed in Sect. 3 (note that when fitting the asymmetry profile, $A(\Delta\lambda)$, we select a wavelength window to exclude the influence of other spectral lines in the wing; while the profile of $I_0(\Delta\lambda)$ is recovered using an extended wavelength window as plotted in Figure 5), and already indicates a sizeable emission compared with the undisturbed profile. This means that the atmosphere below the condensation may also be heated as a consequence through diverse ways, which is in agreement with the flare dynamic models (Fisher et al. 1985; Gan & Mauas 1994). However, we note some difference between Hα and Ca II λ8542, namely, $I_0(\Delta\lambda)$ reveals a central emission peak in the case of Ca II λ8542. The result is

reasonable. The chromosphere, where the core of the Ca II λ8542 line is formed, is heated and condensed during the flaring process, and it induces an enhanced source function in this layer, thus generating the central emission in the absorption line of Ca II λ8542.

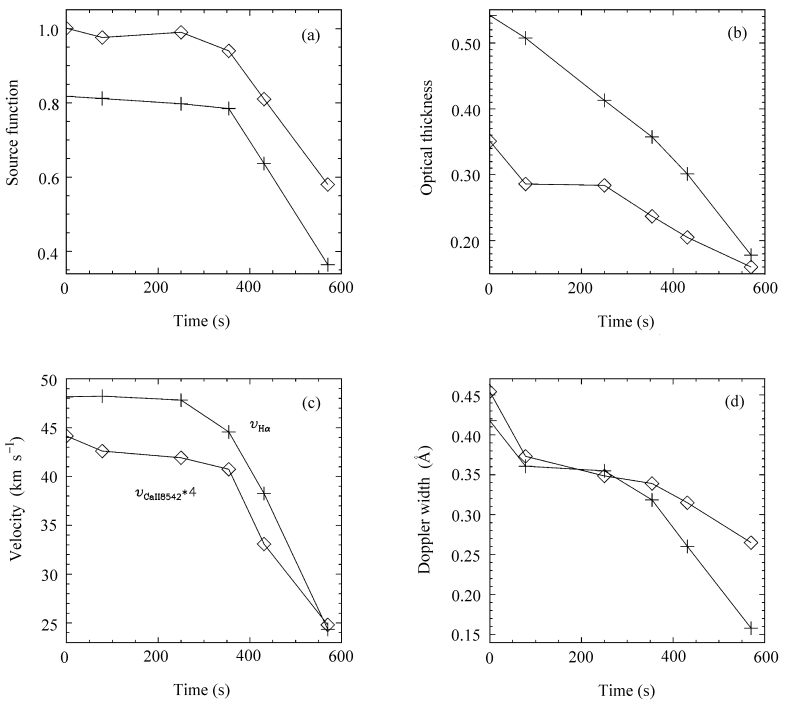

Fig. 4 Temporal variations of the four parameters averaged over the ten brightest pixels within the flare kernels derived from Hα (plus sign) and Ca II λ8542 (diamond) after 02:09:53 UT: (a) source function (in units of I_c near each line); (b) optical thickness; (c) downward velocity; (d) Doppler width. Note that the velocity deduced from Ca II λ8542 is multiplied by a factor of 4.

Another consequence of the condensation is that it is a significant factor in shaping the asymmetry of the observed profile. In the case of Hα, the observed line profile seems to consist of two components: one static and one displaced. The core of the observed profile is generally the center of the static component and has nearly no shift, while the shifted one makes the profile red asymmetric. For the Hα line, the Doppler shift in the downward moving region is much larger than the Doppler width, hence the two parts may become radiatively disconnected. Thus only the red wing of the observed profile exhibits an excess emission while the other parts are almost identical to $I_0(\Delta\lambda)$ (Figure 5, left panel). Contrary to the Hα case, the Ca II λ8542 line shows an obvious excess emission in the central part (Figure 5, right panel). In this case, the Doppler shift is smaller than the Doppler width.

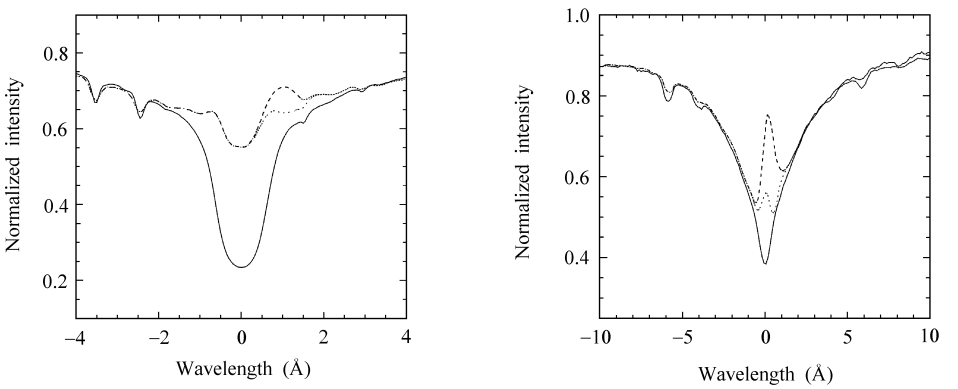

Fig. 5 Comparison of the mean undisturbed profile near the flaring region (solid line), the typical observed profile with red asymmetry (dashed line), and the intensity profile irradiating the perturbed layer from below (dotted line). Left panel for Hα and right panel for Ca II λ8542. The quantities are normalized to the intensity of the adjacent continuum.

It has been found that both the blue and red asymmetries can be caused by downward motions when the condensation is constrained to different heights of the chromosphere (e.g., Gan et al. 1993; Ding & Fang 1996, 1997). It has also been demonstrated that the downflows, driven by the electron beam heating with return current, can produce a blue asymmetry in the Hα line (Heinzel et al. 1994). From the radiation transfer equation, if the source function in the condensation is greater than the underlying intensity irradiating it, the observed profile will exhibit a red asymmetry; otherwise, it displays a blue asymmetry. Actually, the source function we obtained is greater than $I_0(\Delta\lambda)$ in the wavelength window shown in Figure 5 for both the cases of Hα and Ca II λ8542, which is consistent with the fact that the observed profiles are red asymmetric.

5 DISCUSSION

Numerical simulations of flare dynamics show that chromospheric downflows, either caused by heat conduction (e.g., Pallavicini el al. 1983; Cheng et al. 1983; Karpen & DeVore 1987; Gan et al. 1991), or by precipitation of non-thermal electrons (e.g., Livshits et al. 1981; Nagai & Emslie 1984), have similar properties: (1) The chromospheric condensation is geometrically dense and thin, and the velocity is basically constant within it and decreases with time; (2) Velocities ahead of the front of the condensation are zero or negligibly small. These properties validate the adoption of constant parameters throughout the condensation, and confirm the assumption of symmetric background profiles. Based on the precondition, our results are qualitatively consistent with the general framework of flare dynamics.

There is a discrepancy, however, between the observations and the numerical simulations concerning the lifetime of the condensation. Numerical simulations (either thermal or thick-target) predict that the lifetime of the condensation is of the order of 1 min, while from Figure 4c we can find that the velocities derived from Hα remain fairly large even in the later phase. This discrepancy also appeared in previous observations (e.g., Ichimoto & Kurokawa 1984; Ding et

al. 1995) which has been interpreted as a consequence of superposition of several condensations within an unresolved region (Fisher 1989). Recent observations with high time and spatial resolutions have revealed that emissions in the wings of Hα could also exhibit high frequency fluctuations (Wang et al. 2000), which are interpreted as a signature of fine structures related to flare elementary bursts. Ding et al. (2001) have made further explorations through numerical calculations, and found that such fluctuations are probably produced in the chromosphere, which is successively perturbed by short-lived, small-scale injection of high energy electrons. In this scenario, the observed line profile is a convolution of many such spatially unresolved small bursts which are initiated at different times; thus, the net line emission (line integrated intensity with the preflare value subtracted) and the velocity derived from the line could both remain fairly large in the later phase.

To understand the above point more clearly, we choose two small boxes each of area $1.7'' \times 2''$ (see Figure 1, left panel), and plot in Figure 6 the temporal variation of the downward velocity averaged over each small box, as well as the variation of the net line emission of Hα integrated over the line profile. We can find that, for the box B, the net line emission gets some rise in the later phase, and the velocity correspondingly increases; for the box A, the net line emission remains almost constant in the later phase, while also accompanied by a fairly large velocity.

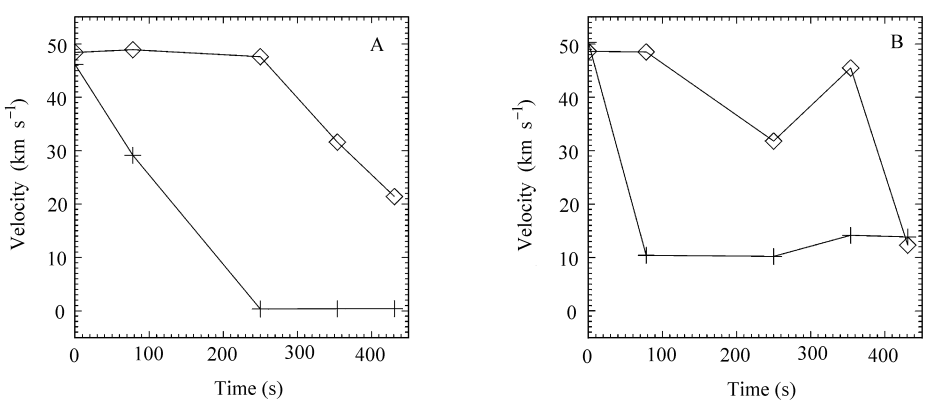

Fig. 6 Temporal variation of the downward velocity (diamond) averaged over the pixels in small box A (left panel) and B (right panel) after 02:09:53 UT. Plus signs mark the variation of the net line emission of Hα (in arbitrary units) integrated over the line profile.

6 CONCLUSIONS

We analyzed multi-line 2D spectra of a flare of 1999 December 22 using a new fitting method, and made a combined discussion on the distributions of physical parameters and their temporal evolutions. The results are as follows:

(1) The spatial properties of the physical parameters derived from Ca II λ8542 over the flare kernels are generally similar to those derived from Hα.

(2) The parameters derived from Hα and Ca II λ8542 show similar temporal evolutions, implying that the two lines may be perturbed by a same heating mechanism and dynamic process.

(3) There is an obvious heating effect on the material below the condensation, which is consistent with the flare dynamic model (Fisher et al. 1985; Gan & Mauas 1994).

(4) It is interpreted and demonstrated in various ways that the red asymmetry of the line profiles is caused by chromospheric downflows of several tens of km s^{-1}. The velocity in the layer contributing to the Ca II λ8542 line emission is about 10 km s^{-1}, much smaller than that deduced from Hα (Liu & Ding 2001).

(5) The downward velocity peaks before the Hα maximum of the flare, and then decays gradually. It remains fairly large even in the later phase, which is interpreted as a consequence of successive elementary flare bursts, i.e., heating by short-lived, small-scale, high energy electrons.

The results derived from multi-line 2D spectra, based on our method, are consistent with the general picture predicted by the flare dynamic models. As pointed out by some authors (e.g., Gan et al. 1991), it will be worthwhile investigating the relation between the Hα line profile and the chromospheric condensation, whereby to provide a theoretical base for the diagnostics of the hydrodynamic process in solar flares from spectral observations. Certainly, a really sophisticated method should be able to match multi-line 2D observations. In this work, we present a new fitting method with which relevant results can be obtained. Therefore, it may provide a useful tool for diagnosing the hydrodynamic process of solar flares.

Acknowledgements The authors would like to express their gratitude to C. Fang and P. F. Chen for valuable suggestions. This work was supported by NSFC and TRAPOYT.

References

Canfield R. C., Galey K. G., 1987, ApJ, 322, 999
Canfield R. C., Metcalf T. R., Strong K. T. et al., 1987, Nature, 326, 165
Cauzzi G., Falchi A., Falciani R. et al., 1996, A&A, 306, 625
Cheng C. C., Oran E. S., Dosceck G. A. et al., 1983, ApJ, 265, 1090
Ding M. D., Fang C., Huang Y. R., 1995, Solar Phys., 158, 81
Ding M. D., Fang C., 1996, Solar Phys., 166, 437
Ding M. D., Fang C., 1997, A&A, 318, L17
Ding M. D., Qiu J., Wang H. M., Goode P. R., 2001, ApJ, accepted
Falchi A., Falciani R., Smaldone L. A., 1992, A&A, 256, 255
Fisher G. H., Canfield R. C., McClymont A. N., 1985, ApJ, 289, 414
Fisher G. H., 1987, Solar Phys., 113, 307
Fisher G. H., 1989, ApJ, 346, 1019
Gan W. Q., Fang C., 1990, Chin. Astron. Astrophys., 14, 413
Gan W. Q., Fang C., Zhang H. Q., 1991, A&A, 241, 618
Gan W. Q., Rieger E., Fang C., 1993, ApJ, 416, 886
Gan W. Q., Mauas P. J. D., 1994, ApJ, 430, 891
Heinzel P., Karlický M., Kotrč P., Švestka Z., 1994, Solar Phys., 152, 393
Huang Y. R., Fang C., Ding M. D. et al., 1995, Solar Phys., 159, 127
Ichimoto K., Kurokawa H., 1984, Solar Phys., 93, 105
Karpen J. T., DeVore C. R., 1987, ApJ, 320, 904
Liu Y., Ding M. D., 2001, Solar Phys., 200, 127
Livshits M. A., Badalyan O. G., Kosovichev A. G. et al., 1981, Solar Phys., 73, 269
Mein P., Mein N., Malherbe J. -M. et al., 1997, Solar Phys., 172, 161
Nagai F., Emslie A. G., 1984, ApJ, 279, 896
Pallavicini R., Peres G., Serio S. et al., 1983, ApJ, 270, 270
Wang H. M., Qiu J., Denker C. et al., 2000, ApJ, 542, 1080